Stem Cell Reports
Article

OPEN ACCESS

Zscan5b Deficiency Impairs DNA Damage Response and Causes Chromosomal Aberrations during Mitosis

Seiji Ogawa,[1,2] Mitsutoshi Yamada,[1,5,*] Akihiro Nakamura,[2] Tohru Sugawara,[2] Akari Nakamura,[2] Shoko Miyajima,[2] Yuichirou Harada,[2] Reina Ooka,[1] Ryuichiro Okawa,[1] Jun Miyauchi,[3] Hideki Tsumura,[4] Yasunori Yoshimura,[1] Kenji Miyado,[2] Hidenori Akutsu,[2] Mamoru Tanaka,[1] Akihiro Umezawa,[2] and Toshio Hamatani[1,5,*]

[1]Department of Obstetrics and Gynecology, Keio University School of Medicine, 35 Shinanomachi Shinjuku-ku, Tokyo 160-8582, Japan
[2]Department of Reproductive Biology, National Research Institute for Child Health and Development, 2-10-1 Ohkura Setagaya-ku, Tokyo 157-8535, Japan
[3]Department of Central Laboratory, Saitama Municipal Hospital, 2460 Midori-ku, Saitama, Saitama-ken 336-8522, Japan
[4]Division of Laboratory Animal Resources, National Research Institute for Child Health and Development, 2-10-1 Ohkura Setagaya-ku, Tokyo 157-8535, Japan
[5]Co-first author
*Correspondence: mitsutoshi.yamada@gmail.com (M.Y.), toshiohamatani@keio.jp (T.H.)
https://doi.org/10.1016/j.stemcr.2019.05.002

SUMMARY

Zygotic genome activation (ZGA) begins after fertilization and is essential for establishing pluripotency and genome stability. However, it is unclear how ZGA genes prevent mitotic errors. Here we show that knockout of the ZGA gene *Zscan5b*, which encodes a SCAN domain with C2H2 zinc fingers, causes a high incidence of chromosomal abnormalities in embryonic stem cells (ESCs), and leads to the development of early-stage cancers. After irradiation, *Zscan5b*-deficient ESCs displayed significantly increased levels of γ-H2AX despite increased expression of the DNA repair genes *Rad51l3* and *Bard*. Re-expression of *Zscan5b* reduced γ-H2AX content, implying a role for *Zscan5b* in DNA damage repair processes. A co-immunoprecipitation analysis showed that *Zscan5b* bound to the linker histone H1, suggesting that *Zscan5b* may protect chromosomal architecture. Our report demonstrates that the ZGA gene *Zscan5b* is involved in genomic integrity and acts to promote DNA damage repair and regulate chromatin dynamics during mitosis.

INTRODUCTION

The occurrence of *de novo* chromosomal abnormalities is a major problem in the use of assisted reproductive technology. Understanding when and how these genomic errors occur is essential to the field of reproductive medicine. In a preimplantation genetic testing for aneuploidies (PGT-A) using 24-chromosome single-nucleotide polymorphisms, approximately 40% of human embryos were found to be aneuploid (Demko et al., 2016). Aneuploidy as a consequence of meiotic chromosome malsegregation is mainly the result of events in oocytes and not spermatocytes: the frequency of maternally derived aneuploidy increases from about 10%–20% to >60% with increasing maternal age (reviewed in Hassold and Hunt, 2001).

Another source of chromosomal anomalies in embryos is postfertilization mitotic division errors that result in embryonic mosaicism (Vanneste et al., 2009). In contrast to meiotic errors, it was found that the incidence of mitotic aneuploidy was not associated with maternal age in either day 3 blastomere biopsies or day 5 trophectodermal biopsies (Capalbo et al., 2013; McCoy et al., 2015). A PGT-A of 28,052 day 3 human embryos indicated that more than 25% harbored aneuploidies of mitotic origin; moreover, the incidence of mitotic aneuploidy exceeded maternally derived meiotic aneuploidy in embryos of women less than 40 years old (reviewed in McCoy, 2017). These mitotic errors produce karyotypically distinct cell lineages within an embryo, which is then termed a mosaic embryo. Mosaicism occurs in ∼15%–90% of all cleavage stage human embryos (Daphnis et al., 2008; Harper et al., 1995; Rubio et al., 2007). Kort et al. (2016) showed that 48% (43/89) of cleavage-stage embryos contained two or more abnormal nuclei; moreover, DNA damage, as indicated by γ-H2AX (phosphorylated [Ser139] histone H2A.X) and replication protein A (RPA) staining, was significantly elevated in cells with micronuclei (74/85, 62/85) compared with cells with normal nuclear morphology (60/642, 36/642) (Kort et al., 2016). Nevertheless, little is known about the molecular basis of mitotic errors and the consequences for mosaic embryonic survival.

After fertilization, the maternal genetic program governed by maternally derived RNAs and proteins is switched to the embryonic genetic program by *de novo* transcription; this switch is termed zygotic genome activation (ZGA) (Hamatani et al., 2004). Nuclear transfer experiments in human somatic cells have demonstrated that ZGA failure can lead to embryonic developmental arrest (Noggle et al., 2011; Yamada et al., 2014). Therefore, ZGA is one of the first and most critical events in animal development. At present two ZGA genes that are specifically expressed during the activation process in embryonic stem cells (ESCs) have been identified, namely, *Zscan4* and *Hmgpi*. *Zscan4* is essential for long-term culture of ESCs and

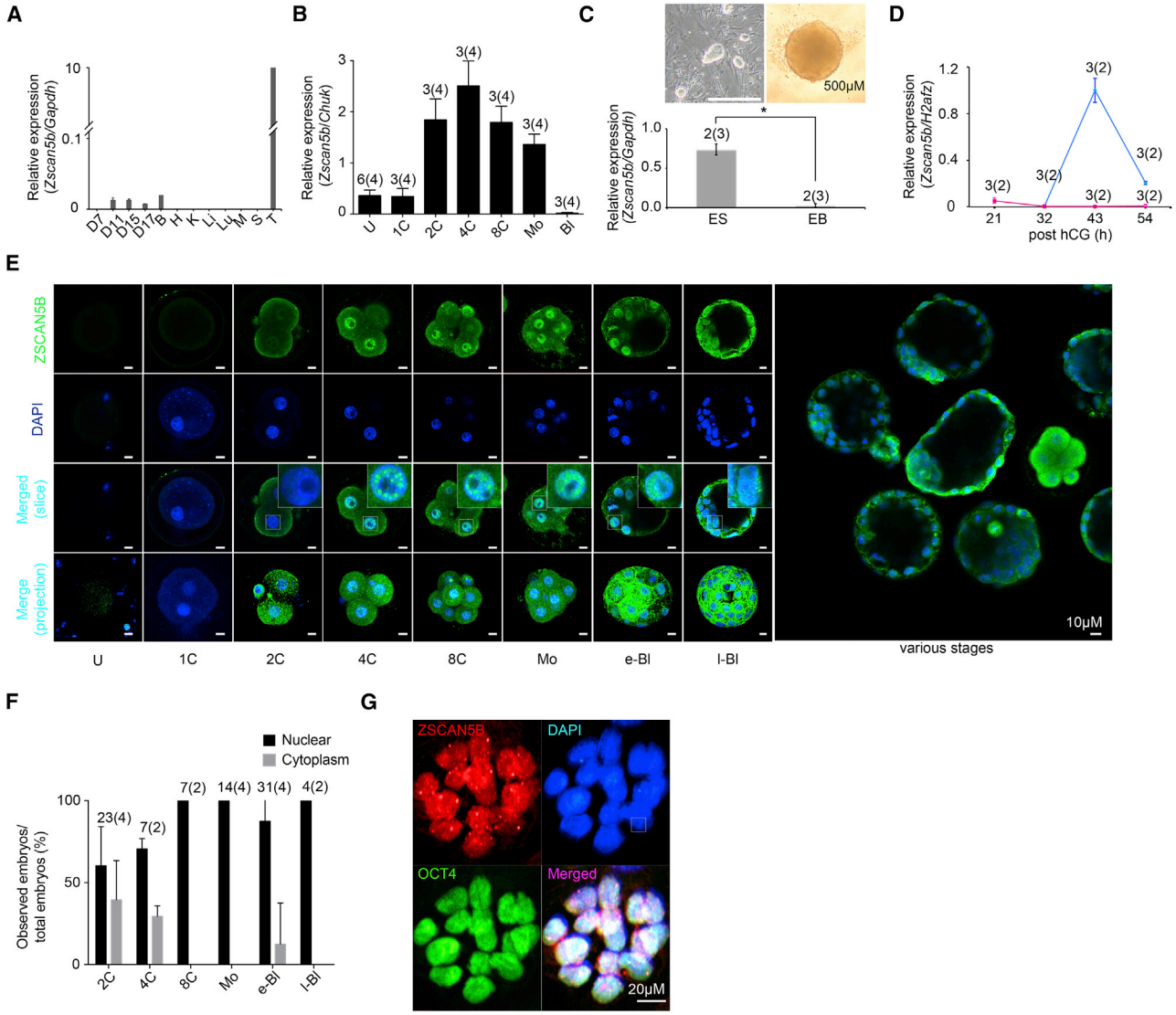

Figure 1. *Zscan5b* Is a Zygotic Genome Activation Gene which Is Specifically Expressed during Preimplantation Stages and in Embryonic Stem Cells

(A) Real-time qPCR analysis of *Zscan5b* expression in adult tissues and during postimplantation development (E7–E17). mRNA was isolated from mouse tissues (B, brain; H, heart; K, kidney; Li, liver; Lu, lung; M, muscle; S, spleen; T, testis). The expression levels were normalized against the reference gene *Gapdh*. Values are means ± SEM from three technical replicates.

(B) Real-time qPCR analysis of *Zscan5b* expression during preimplantation development. Three sets of 10 pooled embryos were collected from unfertilized eggs (U), fertilized eggs (F), two-cell embryos (2), four-cell embryos (4), eight-cell embryos (8), morulae (M), and blastocysts (B) are shown after normalization to an internal reference gene (mouse *Chuk*). Values are means ± SEM from four separate experiments. The total number of samples and the number of individual experiments (in parentheses) contributing to a particular experiment are indicated above each column.

(C) *Zscan5b* is transcribed in embryonic stem cells (ESCs), but not in differentiated embryoid bodies (EBs). The expression levels were normalized against the reference gene *Gapdh*. Values are means ± SEM from three separate experiments. The total number of samples and the number of individual experiments (in parentheses) contributing to a particular experiment are indicated above each column.

(D) *De novo* (zygotic) transcription of the *Zscan5b* gene. Application of α-amanitin, an RNA polymerase II inhibitor, showed that *Zscan5b* is transcribed zygotically, but not maternally. *Zscan5b* expression was not observed before the two-cell stage, and α-amanitin completely inhibited *de novo* transcription at the two-cell stage. The expression levels were normalized using *H2afz* as a reference gene. Values are means ± SEM from two separate experiments. The total number of samples and the number of individual experiments (in parentheses) contributing to a particular experiment are indicated above each column.

(legend continued on next page)

maintenance of chromosomal integrity during telomere elongation (Falco et al., 2007; Zalzman et al., 2010). *Hmgpi* is responsible for DNA replication and has a role in peri-implantation development and ESC isolation (Yamada et al., 2010).

Another ZGA gene, *Zscan5b*, is predicted to encode a SCAN domain with C2H2 zinc fingers (C2H2-ZF). Zinc-finger genes represent a significant portion of the genes in the vertebrate genome (reviewed in Edelstein and Collins, 2005). The DNA-binding sites, interacting proteins, and transcriptional responses to genetic perturbation of C2H2-ZF proteins have recently been characterized (Schmitges et al., 2016). The SCAN domain, a leucine-rich region, functions as a protein interaction domain that mediates self-association or selective association with other proteins (Edelstein and Collins, 2005). These structural characteristics suggest that *Zscan5b* plays a role in genomic stability either independently or in combination with other factors for telomere elongation, such as *Zscan4* (Zalzman et al., 2010), or for apoptosis-dependent DNA damage response, such as *Zscan10* (Skamagki et al., 2017).

Although the origins of chromosomal abnormalities are well documented in the literature and are known to contribute to female infertility, the molecular mechanisms of these abnormalities are not well understood. In the present study, we hypothesized that the ZGA gene *Zscan5b* is involved in genome stability during mitosis. We tested this hypothesis by determining whether *Zscan5b*-deficient mice could act as a model for spontaneous mitotic chromosomal errors, and also investigated the roles of this ZGA gene in genome stability after fertilization and in developmental competency. Our analyses show that *Zscan5b* deficiency causes chromosomal abnormalities, and leads to the growth of early-stage cancerous lesions.

RESULTS

Gene Structure and Expression of the ZGA Gene *Zscan5b*

An *in silico* analysis showed that mouse *Zscan5b* was expressed specifically in preimplantation embryos. Gene expression profiling indicated that *Zscan5b* transcript levels were upregulated during ZGA at the one- to four-cell embryo stages (Boroviak et al., 2018; Hamatani et al., 2004; Wang et al., 2004) (Figures S1A and S1B). RNA sequencing analysis of preimplantation embryos indicated that human *ZSCAN5B* levels peaked at the eight-cell stage (Figure S1C) (Boroviak et al., 2018), suggesting that human *ZSCAN5B* is also transcribed zygotically during the major burst of ZGA. Three primate-specific paralogs, *ZSCAN5A*, *ZSCAN5C*, and *ZSCAN5D*, have been identified that are divergent from the parental gene (Sun et al., 2016); the level of primate ZSCAN5A peaked at the eight-cell stage (Figure S1D) (Boroviak et al., 2018). Analysis of a public expressed sequence tag (EST) database identified 21 cDNA clones that were found exclusively in preimplantation embryos (two-cell to morula stages) (Figure S1E). One of these clones (AK13965.1) contained the full *Zscan5b* gene coding sequence, which spans 1,980 bp and has 2 exons; SMART domain prediction analysis indicated the gene encodes a putative protein of 468 amino acids (NP_001028965.1) that harbors a SCAN domain and five zinc-finger domains (Schultz et al., 1998) (Figure S1F). In the NCBI Gene database, the *Zscan5b* gene has three transcripts (splice variants). Two of three splice variants contain a full-length open reading frame encoding a single protein model. The *Zscan5b* gene is predicted to be conserved in *Homo sapiens*, and pairwise alignment scores by a BLAST search of amino acid sequences for the human ortholog indicated 54% similarity (Figure S1G).

Experimental analyses were carried out to confirm the results of the *in silico* analysis that indicated a preimplantation stage-specific expression pattern for *Zscan5b*. A real-time PCR analysis using cDNA isolated from mouse adult tissues and fetuses (embryonic day [E]7, E11, E15, and E17) detected *Zscan5b* expression in all tested tissues (Figure 1A). Real-time qPCR analysis of preimplantation embryos indicated that *Zscan5b* mRNA levels increased during the one- to two-cell stages, peaked at the four-cell stage, and then gradually decreased during the eight-cell to blastocyst stages (Figures 1B, S1H, and S1I). The real-time qPCR results were separately normalized against the internal standard genes *Chuk*, *H2afz*, and *Gapdh* (Falco et al., 2006; Mamo et al., 2007) to ensure their reproducibility. The normalization procedure confirmed the *in silico* prediction of a preimplantation stage-specific expression pattern of *Zscan5b*. Expression of *Zscan5b* was found in isolated mouse ESCs, whereas it was downregulated in differentiated tissues

(E) Immunocytochemical analysis of ZSCAN5B expression. Preimplantation embryos were immunostained with an anti-ZSCAN5B antibody (green). Nuclei are shown by DAPI staining (blue). ZSCAN5B protein was detected throughout the preimplantation embryo stages. Scale bars represent 10 μm.

(F) Nuclear translocation of ZSCAN5B protein during preimplantation development. ZSCAN5B was mainly detected in the nucleus of preimplantation embryos. Nuclei are shown by immunostaining with DAPI staining (blue). The total number of samples and the number of individual experiments (in parentheses) contributing to a particular experiment are indicated above each column.

(G) ESC colony stained with antibodies against *Zscan5b* (red) and *Oct4* (green), and with DAPI. ZSCAN5B is distributed as dot-like foci in the nucleus, in contrast to the pattern by ZSCAN4 (Falco et al., 2007).

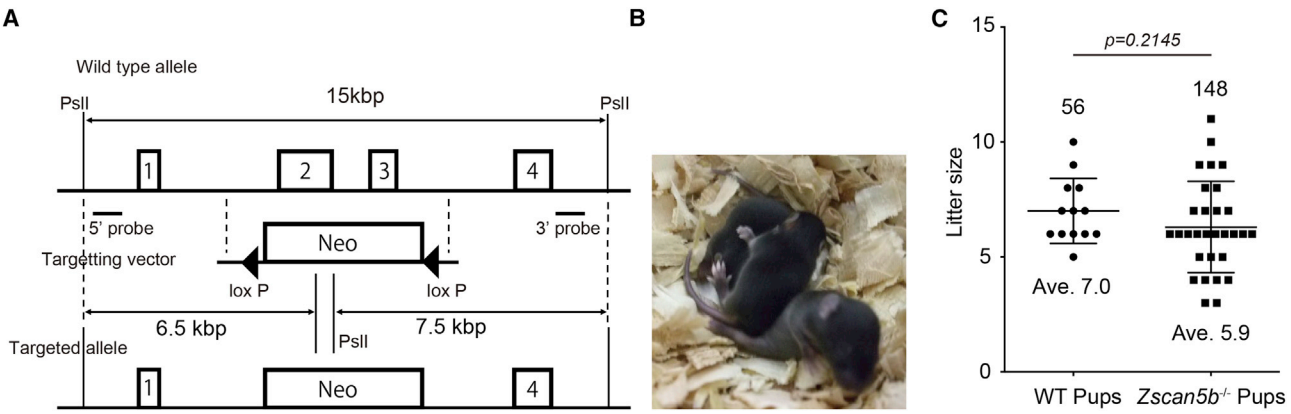

Figure 2. Differential Potential of *Zscan5b*-Deficient Mice and Embryos Derived from *Zscan5b*-Deficient ESCs

(A) Chimeras generated by injection of *Zscan5b* heterozygous ESCs into ICR host blastocysts.

(B) *Zscan5b*-deficient mice.

(C) Average litter size of *Zscan5b*-deficient mice compared with wild-type mice (p = *0.2145*).

(embryoid bodies) (Figure 1C). We then performed real-time qPCR analysis using α-amanitin, an RNA polymerase II inhibitor, to investigate *de novo* (zygotic) transcription of the *Zscan5b* gene. The presence of α-amanitin during *in vitro* culture from the one-cell stage significantly reduced *Zscan5b* mRNA expression in embryos at 43 and 53 h post-human chorionic gonadotropin (hCG) (early and late two-cell stages, respectively) (Figure 1D), suggesting that *Zscan5b* is transcribed zygotically during the major burst of ZGA. Our results contradict a previous report showing ubiquitous expression of *Zscan5b* (Sun et al., 2016), although both studies detected high expression in early embryos and in the testis.

Level of the ZSCAN5B Protein

To study the temporal and spatial distribution of the protein (ZSCAN5B) encoded by *Zscan5b* in mice, we raised a polyclonal antibody against ZSCAN5B peptides. Our gene expression analysis indicated that *Zscan5b* transcription started at the two-cell stage, peaked at the four-cell stage, and then gradually decreased until the blastocyst stage (Figure 1E); immunostaining with the polyclonal antibody showed the presence of ZSCAN5B from the two-cell stage until the blastocyst stage. ZSCAN5B was also present in both inner cell mass cells and trophectodermal cells of blastocysts.

ZSCAN5B was detected in the cell nucleus and cytoplasm throughout the preimplantation development (Figures 1E and 1F); however, it was exclusively localized to nuclei in eight-cell, morula, and late-blastocyst stages. ESCs isolated from blastocyst embryos were ZSCAN5B positive, with distribution mainly restricted to the nucleus, suggesting a specific role as a nuclear protein in preimplantation embryos and ESCs (Figure 1G). We also found that the OCT4 protein colocalized with ZSCAN5B in the nucleus of ESCs (Figure 1G). These results indicate that ZSCAN5B is a putative nuclear protein.

Zscan5b Is Not Essential for Fertility

Our *in silico* analysis demonstrated that the *Zscan5b* gene consisted of seven exons (Figure S1F). To investigate the function of the ZSCAN5B protein in ESCs, we constructed a plasmid, pNT1.1, carrying a modified *Zscan5b* sequence in which the second and third exons were replaced with a neomycin resistance cassette (*Neo*) (Figure 2A). The construct was introduced into C57BL/6 mouse ESCs by electroporation, and colonies with resistance to the drug G-418 were screened for homologous recombination. Using the *Neo* targeting vector, 192 colonies were screened by Southern blotting (data not shown), and 14 (7.3%) heterozygous ESCs were isolated. To study the *in vivo* function of *Zscan5b*, we injected five *Neo* heterozygous ESC lines into C57BL/6 blastocysts. Germline transmission was obtained from three independent ESC clones. Among 64 mice born from heterozygous intercrosses, 12 were wild-type, 27 were heterozygous, and 24 were homozygous. Litter sizes of the intercrossed homozygotes were not significantly lower than those of wild-type mice (Figures 2B and 2C). And intercrossed homozygous mice produced second-generation homozygotes.

Zscan5b Is Not Essential for Acquiring Self-Renewal Potential in the Derivation of ESCs

To identify ESCs homozygous for the introduced gene mutation, blastocysts were tested in an outgrowth assay. *Zscan5b*-deficient embryos showed vigorous outgrowth, leading to the derivation of ESCs that were alkaline phosphatase (ALP) positive (Figure 3A). Thirteen *Zscan5b* homozygous ESC lines were isolated, and these clones were confirmed

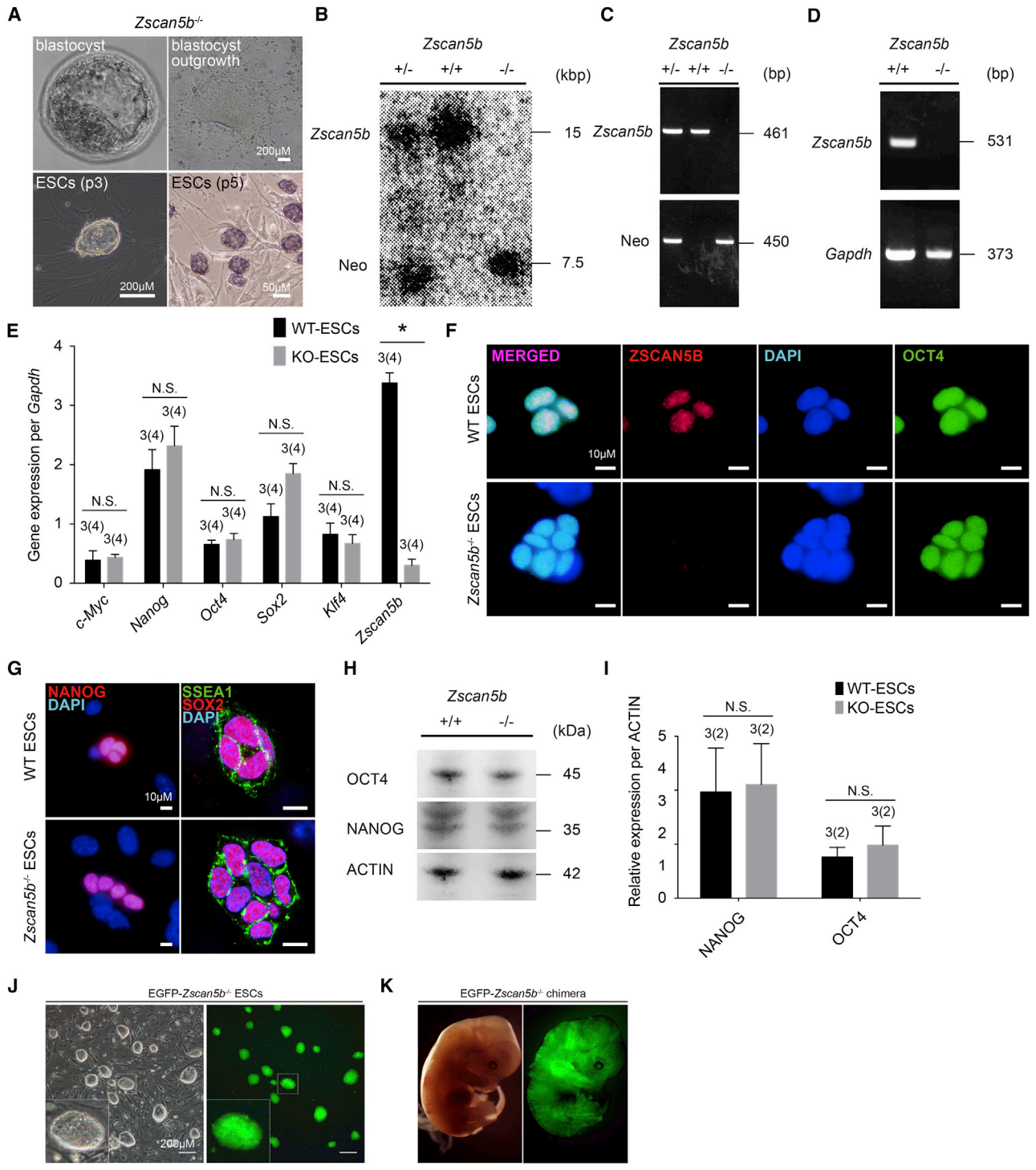

Figure 3. Expression of Pluripotency Markers in *Zscan5b*-Deficient ESCs Is Comparable with Wild-Type ESCs

(A) A *Zscan5b*-deficient blastocyst and blastocyst outgrowth are shown in the upper panel. Morphological appearance of *Zscan5*-deficient ESCs and ALP staining (purple) of *Zscan5b*-deficient ESCs are shown in the lower panel. Scale bars represent 200 and 50 μm.

(B and C) Southern blotting analysis-based genotyping (B) and PCR-based genotyping (C) to distinguish between wild-type, *Zscan5b* heterozygous (+/−) and *Zscan5b*-deficient (−/−) ESCs.

(D) Reverse transcription PCR analysis of *Zscan5b* mRNA expression in wild-type and *Zscan5b*$^{-/-}$ ESCs.

(legend continued on next page)

to be homozygous for the *Zscan5b* mutation by Southern blotting (Figure 3B) and genomic PCR (Figure 3C). Revserse transcription PCR and real-time qPCR analysis further confirmed the lack of *Zscan5b* expression in homozygous cells (Figures 3D and 3E). All of these cell lines were positive for pluripotency markers (Figures 3E–3I). To test whether *Zscan5b* contributes to normal development, a chimera assay was performed; this assay indicated that *Zscan5b*-deficient ESCs could contribute to the whole body (Figures 3J and 3K). These results suggest that *Zscan5b* does not contribute to ESC derivation or stemness as pluripotent stem cells.

Differentiation Assays *In Vitro* and *In Vivo*

In embryoid bodies, *Zscan5b*-deficient ESC lines gave rise to cell types in all three germ layers (Figure 4A). Surprisingly, on transplantation into immunocompromised mice, all *Zscan5b* homozygous ESC lines developed small malignant germ cell tumors (Figure 4B). The tumors primarily exhibited the histology of mature teratomas, and consisted of tridermic elements, with scattered foci of immature teratomas mainly consisting of neural tissues. Furthermore, adjacent to the immature teratoma components, a small number (1–3 per tumor) of tiny foci with malignant germ cell tumor components, histologically distinct from the immature teratoma cells, were present. The size of these lesions ranged from 0.5 to 3 mm in diameter, with most being around 1 mm. We classified these lesions as choriocarcinomas and embryonal carcinomas. However, the very small sizes and the multiplicity of these apparently malignant germ cell tumor components, in addition to the absence of metastatic lesions outside the tumor, might indicate that they were very early-stage cancerous lesions rather than authentic, fully malignant germ cell tumors with metastasizing potential. The tumor sizes developed from *Zscan5b*-deficient ESC lines was comparable with that from wild-type ESC lines (Figures 4C and 4D).

DNA Repair Is Mediated through *Zscan5b*

The mechanisms underlying the tumorigenic characteristics of *Zscan5b*-deficient ESCs were investigated by X-irradiating the cells and staining for the DNA damage markers γH2AX and RPA. γH2AX foci in nuclei were significantly more frequent in *Zscan5b*-deficient ESCs than in wild-type ESCs (Figures 5A and 5B). Also, the number of foci of RPA, a single-strand DNA-binding protein, in *Zscan5b*-deficient ESCs was increased (not significantly) (Figures 5C and 5D), indicating the presence of DNA damage such as DNA double-strand breaks during mitosis.

Global transcriptional changes, including those of DNA repair genes, were investigated in a microarray analysis of three wild-type ESC lines and three *Zscan5b*-deficient ESC lines (Tables S2 and S3). Using a clustering analysis, we found that the *Zscan5b*-deficient ESC lines grouped separately from the wild-type ESC cell lines (Figures 5E and 5F). In addition, all three *Zscan5b*-deficient ESC lines showed elevated expression of the DNA damage repair genes *Rad51l3* and *Bard1* (Table S2), indicating that *Zscan5b* deficiency induces susceptibility to DNA damage.

To determine whether DNA damage repair depends on *Zscan5b*, a piggyBac vector carrying wild-type *Zscan5b*-GFP driven by a CAG promoter for long-term stable expression was transfected into *Zscan5b*-deficient ESCs. We found a significant increase in DNA damage after irradiation in *Zscan5b*-deficient ESCs. However, a lower frequency of γH2AX foci was present in transfected *Zscan5b*-deficient ESCs (Figures 5G–5I), suggesting that restoration of *Zscan5b* expression in these cells was sufficient to restore genome stability. Therefore, we conclude that DNA damage can be resolved through *Zscan5b*-dependent repair pathways.

Zscan5b Deficiency Increases Chromosomal Aberrations

Chromosome instability is a feature of many cancers and may be a crucial factor in carcinogenesis. We carried out a chromosomal analysis of *Zscan5b*-deficient ESCs and somatic cells of homozygous-deficient adult mice. Analysis of Q-banded chromosomes showed that they displayed an increasing number of chromosome breaks, defined as a disruption in the chromosome, in *Zscan5b*-deficient ESCs (Figures 6A, 6B, and S3). Fusion of chromosome

(E) Real-time qPCR analysis of *c-Myc*, *Nanog*, *Oct4*, *Sox2*, *Klf4*, and *Zscan5b* in wild-type and *Zscan5b*$^{-/-}$ ESCs. The cell line number is shown above each bar, and the number shown in the parentheses indicates four independent experiments. Error bars, SEM. N.S., not significant.
(F and G) Immunofluorescence staining for (F) ZSCAN5B (red) and OCT4 (green), (G) NANOG (red), SSEA1 (green), and SOX2 (red) in wild-type and *Zscan5b*$^{-/-}$ ESC colonies as observed under confocal microscopy. Nuclei are stained with DAPI (blue). Scale bars represent 10 μm.
(H and I) Immunoblot analysis of OCT4 and NANOG in wild-type and *Zscan5b*$^{-/-}$ ESCs (H). The expression levels were normalized using actin expression (42 kDa) as a reference (I). The observed cell line number is shown above each bar, and the number shown in the parentheses indicates two independent experiments. Error bars, SEM. N.S., not significant.
(J) Fluorescence microscopic images of EGFP-*Zscan5b*-deficient ESC colonies. These ESC colonies showed constitutive expression of EGFP. Scale bars represent 200 μm.
(K) EGFP-*Zscan5b*-deficient chimera mouse. Fluorescence stereomicroscopic image of an embryo at E12.5 generated from blastocysts injected with EGFP-*Zscan5b*-deficient ESCs. The contribution of EGFP-*Zscan5b*-deficient ESCs was detected throughout the whole body.

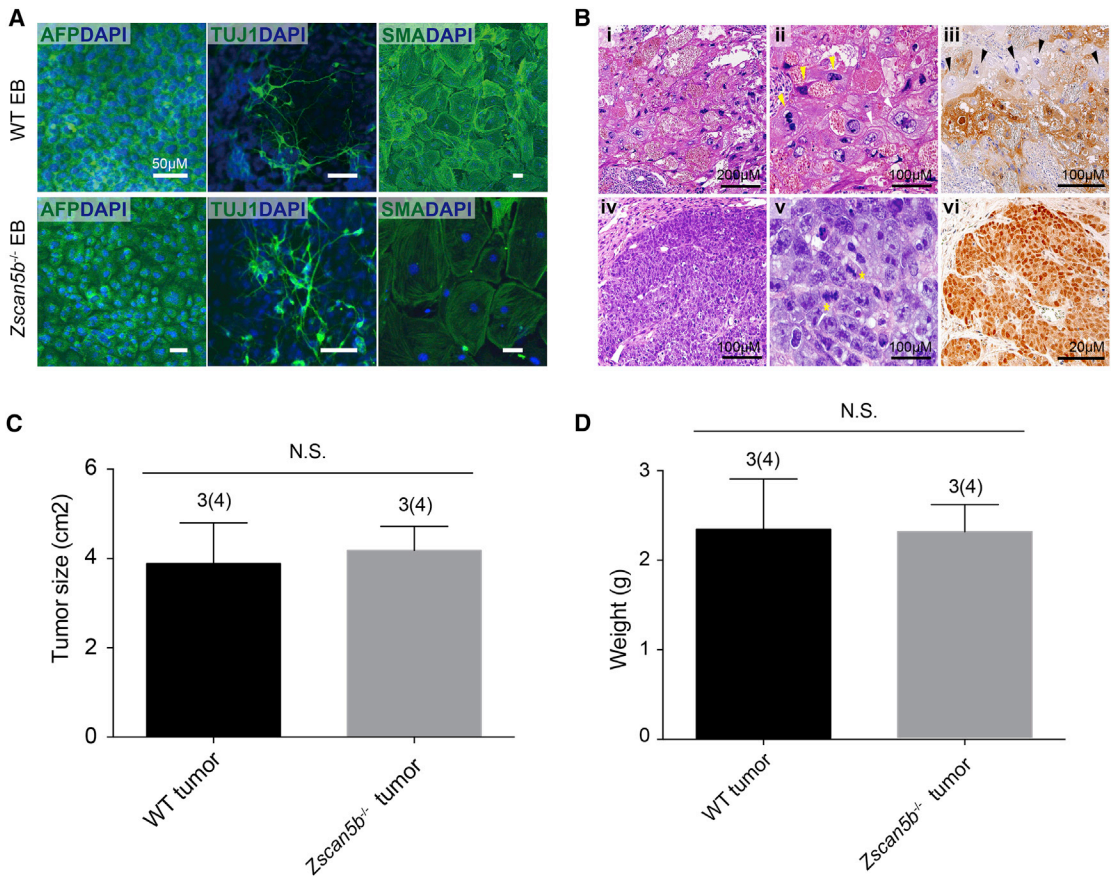

Figure 4. Injection of *Zscan5b*-Deficient ESCs Results in the Growth of Very Early-Stage Cancerous Lesions

(A) Embryoid bodies (EBs) differentiated from *Zscan5b*-deficient ESCs are stained with AFP (green), TUJ1 (green), and SMA (green), respectively. Nuclei are stained with DAPI (blue). Scale bars represent 50 μm.

(B) Teratoma formation assay. (i–iii) Choriocarcinoma. (i) Low-power micrograph shows a hemorrhagic lesion with large, atypical trophoblastic cells. (ii) Higher magnification reveals two types of cell, namely, cytotrophoblast-like cells (white arrowhead) and syncytiotrophoblasts (yellow arrowhead). (iii) Immunohistochemistry for hCG demonstrates positive staining in the latter type of cells, whereas the former type is negative (arrowhead). (iv–vi) Embryonal carcinoma. (iv) Low-power micrograph shows an alveolar structure consisting of solid sheets of monotonous atypical cells. (v) Higher magnification reveals cohesive cells with indistinct cytoplasmic border and large nuclei with prominent nucleoli, characteristic features of embryonal carcinomas. Many mitotic figures are seen (asterisk). (vi) Immunohistochemistry for OCT4 demonstrates positive staining in the nuclei of the tumor cells. Scale bars, 200 μm (i), 100 μm (ii–iv, vi), and 20 μm (v).

(C and D) Tumor sizes (C) and weights (D) derived from *Zscan5b*-deficient ESCs are comparable with teratomas from wild-type ESCs. Error bars, SEM. N.S., not significant.

fragments and unrepaired chromosome breaks are known to be associated with cell malignancy (reviewed in van Gent et al., 2001). Somatic cells from *Zscan5b*-deficient adults showed chromosome instability with a significantly increased frequency of chromosome gaps, derivative chromosomes, gain or loss of chromosomes, Robertsonian translocations, and chromosome breaks (Figure S4). In particular, the frequency of chromosome gaps in spleen cells of the *Zscan5b*-deficient mice was significantly higher than in those of wild-type mice (43.0% versus 1.3%, $p < 0.001$). The positions of chromosome gaps were random in all chromosomes except chromosome 11 (Figures S3 and S4; Table S4). These results imply that *Zscan5b* deficiency can lead to chromosome instability and stochastically derived chromosome gaps may induce other chromosomal abnormalities such as chromosome breaks.

ZSCAN5B Binds to Histone H1

From the results of our various analyses, we propose that *Zscan5b* likely protects cells against a range of *de novo* chromosomal abnormalities during mitosis. We further speculate that ZSCAN5B binds either directly or indirectly to

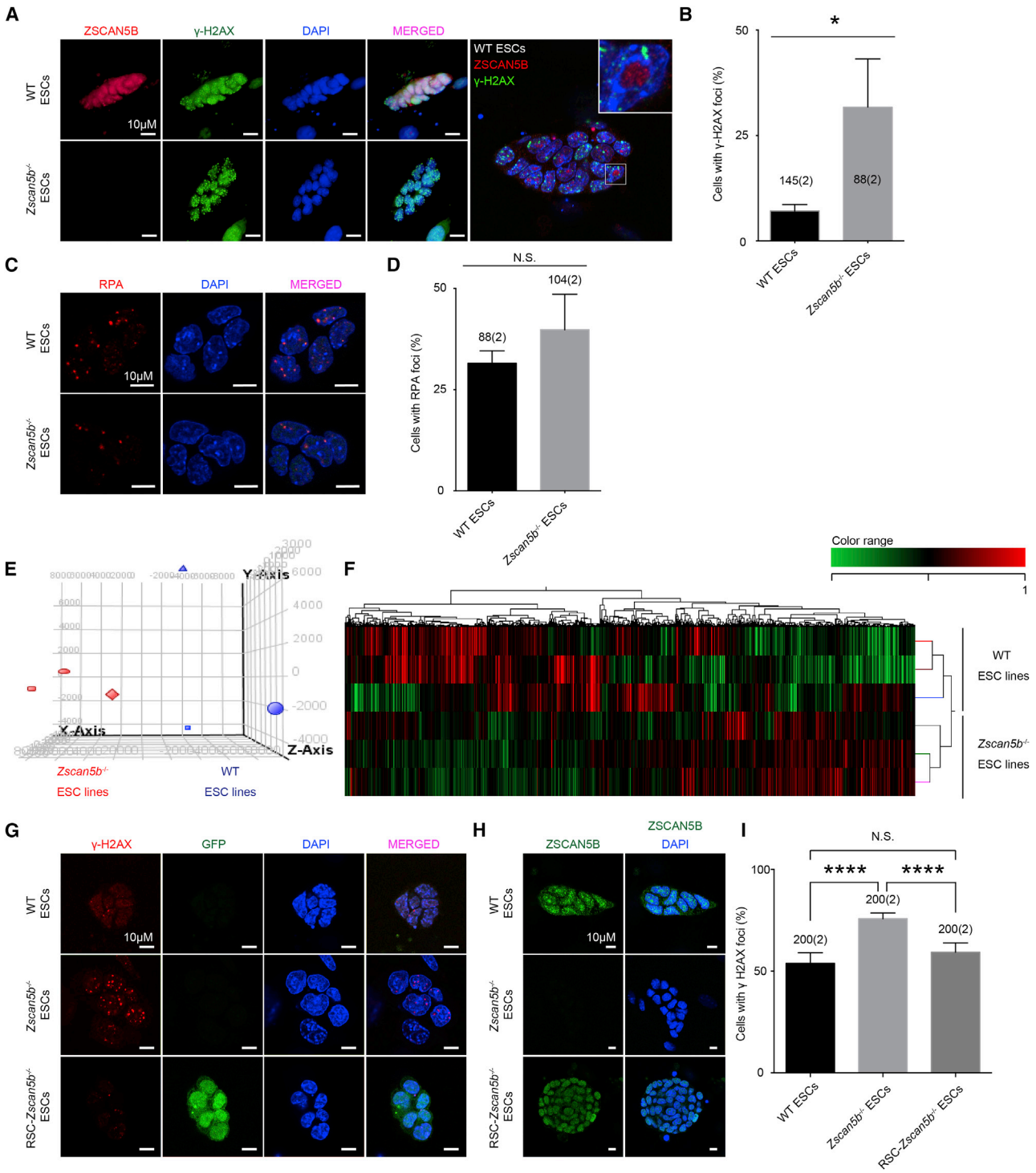

Figure 5. Genomic Instability in *Zscan5b*-Deficient Cells

(A and B) Immunostaining for γ-H2AX indicating DNA damage (A) and mean γ-H2AX-positive foci (B) in irradiated *Zscan5b*-deficient ESCs. Scale bars represent 10 μm. The number of analyzed cells is shown above each bar, and the number shown in the parentheses indicates two independent experiments. Error bars, SEM.

(C and D) Immunostaining for RPA (C) and mean RPA-positive foci (D) in *Zscan5b*-deficient irradiated ESCs. Scale bars represent 10 μm. The number of analyzed cells is shown above each bar, and the number shown in the parentheses indicates two independent experiments. Error bars, SEM. N.S., not significant.

(legend continued on next page)

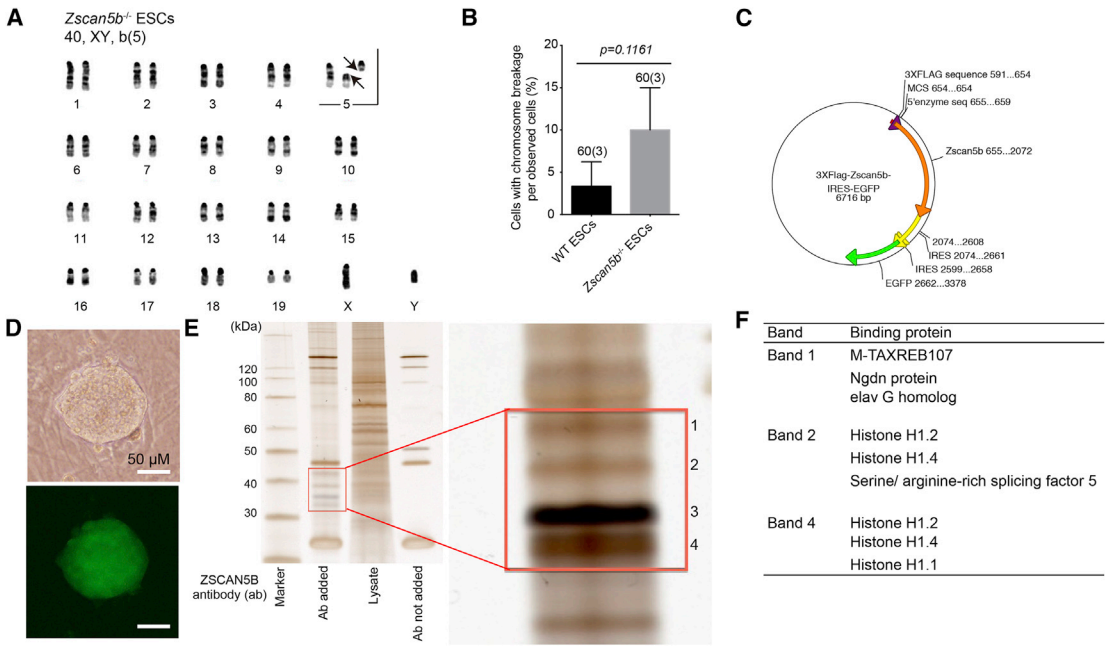

Figure 6. ZSCAN5B Binds to Histone H1

(A and B) Chromosome breaks in *Zscan5b*-deficient ESCs (A). The error bars indicate SEM of two replicates of each cell line (B). The image shown in (A) is also shown in Figure S3D.

(C) IRES-EGFP vector of the *Zscan5b*$^{-/-}$.

(D) The vector transfected into ESCs (upper panel) expresses GFP (lower panel). Scale bars represent 50 μm.

(E) Analytical gel electrophoresis of anti-Flag antibody-conjugated proteins extracted from ESCs. The gel was stained with the SilverQuest Silver Staining Kit (Invitrogen).

(F) Liquid chromatography-mass spectrometry analysis of targeted bands 1, 2, and 4. ZSCAN5B binds to proteins of the histone H1 family.

chromosomes, and helps to form nucleosome structures. To test these speculations, we performed a co-immunoprecipitation analysis using protein extracted from ESCs transfected with 3XFLAG-Zscan5b-EGFP (Figures 6C–6E). The components of bands from 3XFLAG-Zscan5b-EGFP combined proteins were analyzed and the histone H1 family, H1.1, H1.2, and H1.4, was specifically detected in bands 1, 2, and 4 of the antibody-added protein samples (Figure 6F). We cross-validated these results by an immunoprecipitation assay using cells transfected with a pcDNA3.1+C-eGFP plasmid carrying mouse *Zscan5b* cDNA and three pcDNA3.1-MYC-HIS A plasmids carrying mouse histone 1,1, 1.2, and 1.4 cDNAs (Figure S5). The sizes of the bands corresponded to the molecular sizes of histones H1.1, H1.2, and H1.4 in the antibody-added protein sample. These results support our suggestion that ZSCAN5B binds to histones H1.1, H1.2, and H1.4.

DISCUSSION

Here we have demonstrated that a ZGA gene, *Zscan5b*, contributes to the maintenance of DNA integrity against cellular DNA damage and *de novo* chromosomal aberrations during mitosis, thereby preventing development of cancers. *Zscan5b*-deficient ESCs did not differ from wild-type

(E) Principal-component analysis of global gene expression patterns of *Zscan5b*$^{-/-}$ ESC lines (shown in red) and wild-type ESC lines (blue).

(F) Heatmap of most highly up- or downregulated genes in *Zscan5b*$^{-/-}$ ESC lines in comparison with the control wild-type ESC lines and cluster diagram of global gene expression profile of *Zscan5b*-deficient ESC lines in comparison with the control wild-type ESC lines. Shown are the microarray expression ratios of each sample relative to the mean in the ESC samples (in a logarithmic scale). The red and green color ranges denote at least a 2-fold change.

(G–I) Immunofluorescence staining for γ-H2AX (red) and GFP (green) (G), and ZSCAN5B (H) of wild-type irradiated ESCs, *Zscan5b*-deficient irradiated ESCs, *Zscan5b* rescued *Zscan5b*-deficient irradiated ESCs, and mean γ-H2AX-positive foci (I). Nuclei are stained for DAPI (blue). Scale bars represent 10 μm. The number of analyzed cells is shown above each bar, and the number shown in the parentheses indicates two independent experiments. Error bars, SEM. N.S., not significant.

ESCs in terms of pluripotency but did display a distinct range of abnormalities including elevated DNA stress and chromosomal abnormalities. Interestingly, spleen cells isolated from *Zscan5b*-deficient adult mice showed random distribution of gaps in their chromosomes; gaps were defined here as an unstained section in a chromatid. A co-immunoprecipitation analysis showed that ZSCAN5B bound to the linker protein histone H1, suggesting a role in chromatin dynamics during mitosis. Therefore, the *Zscan5b* gene can be classified as encoding a protein directly involved in DNA repair and protection of chromosomal architecture, and which contributes to preventing the formation of cancerous lesions.

ZSCAN Family Might Contribute to the Maintenance of Genomic Integrity

Nuclear reprogramming during the preimplantation developmental period is crucial for genomic integrity. Although induced pluripotent stem cells (iPSCs) have similar pluripotency to ESCs, those derived from aged donors (A-iPSCs) show diminished DNA damage responses and a defect in the apoptotic response to DNA damage; as a consequence, A-iPSCs show a greater number of cells with genetic abnormalities (Skamagki et al., 2017). Somatic cell nuclear transfer (SCNT) has shown that oocytes can reprogram somatic cells into pluripotent stem cells. Unlike A-iPSCs, stem cells derived by SCNT (ntESCs) using the genome of an aged donor and cytoplasm of a young donor (A-ntESCs) show normal DNA damage responses and normal genomic integrity (Skamagki et al., 2017). The key difference here is that there are more reprogramming factors stored in oocytes; moreover, ZGA genes, including *Zscan5b*, are transcribed more efficiently during preimplantation embryo development than the four "Yamanaka" factors (OCT4, SOX2, KLF4, and c-MYC) (Egli et al., 2008).

Another ZSCAN family gene, *ZSCAN10*, is specifically expressed in ESCs and iPSCs, and higher expression is shown in iPSCs from younger donors (Y-iPSCs) than in A-iPSCs. Overexpression of *ZSCNA10* in conjunction with the four Yamanaka factors can restore impaired genomic integrity in A-iPSCs (Skamagki et al., 2017), implying that *ZSCAN10* is responsible for the poor DNA damage response and genomic instability in A-iPSCs. Although it is unclear whether ZSCAN family genes interact with each other, overexpression of the zygotic gene *Zscan5b* could play a role in restoring genome integrity through DNA repair after the initial DNA damage response in A-iPSCs similar to that in A-ntESCs, as shown here in the rescue experiments.

Origins of Chromosome Abnormalities in *Zscan5b*-Deficient Somatic Cells

A clue to the origin of chromosome abnormalities in *Zscan5b*-deficient somatic cells can be obtained from the consequences of nuclear translocation of the ZSCAN5B protein. Our immunocytological analysis showed that the ZSCAN5B protein was present in both nuclei and cytoplasm at early preimplantation stages, but became predominantly localized to the nucleus from the eight-cell stage. Although the peptide antibody raised against synthetic peptides of ZSCAN5B did not demonstrate high specificity (Figures S2A and S2B), a bipartite nuclear localization signal peptide (RFQCTECKKSFLYKSRFDLHQRSHTGERPFKCILC) was present in the ZSCAN5B sequence based on the *in silico* analysis (Kosugi et al., 2009). Thus, the nuclear localization of ZSCAN5B after the eight-cell stage implies a spatial requirement. The precise timing of formation of chromosomal abnormalities is unclear. Chromosome breaks were observed in one of the three *Zscan5b*-deficient ESC lines isolated from the inner cell mass of *Zscan5b*-deficient blastocysts. In addition, spleen cells from *Zscan5b*-deficient mice showed a range of chromosomal abnormalities. These observations imply that formation of chromosomal abnormalities is initiated from the peri-implantation period. Because chromosome fragments can induce other chromosome aberrations (reviewed in van Gent et al., 2001), these abnormalities might be accumulated during mitosis without *Zscan5b* expression.

Zscan5b Works as a DNA Damage Repair Gene

Zscan5b-deficient ESCs differentiated into germ cell tumors with multilineage, differentiated cell types. Karyotype analysis of ESCs and spleen cells of *Zscan5b*-deficient adults identified chromosomal abnormalities, ranging from small insertions or deletions to large chromosomal alterations. The frequency of γ-H2AX foci in *Zscan5b*-deficient irradiated ESCs was significantly elevated compared with wild-type ESCs. *Zscan5b*-deficient irradiated ESCs also displayed a trend to increased frequency of RPA foci. RPA relocates into distinct nuclear foci and colocalizes with γ-H2AX at the sites of DNA damage in a time-dependent manner (Balajee and Geard, 2004). These results suggest that DNA repair processes after the initial DNA damage response do not work in *Zscan5b*-deficient ESCs. However, our rescue experiment showed the presence of a lower frequency of γH2AX foci (Figures 5H and 5I), suggesting that restoration of *Zscan5b* expression in *Zscan5b*-deficient ESCs was sufficient to restore genome stability. A global transcriptional analysis showed elevated expression of *Rad51l3* and *Bard1* in *Zscan5b*-deficient ESCs (Table S2). RAD51 is a key component of the homologous recombination mechanism of DNA damage repair and is associated with the activation of double-strand break DNA repair (Forget and Kowalczykowski, 2010). BRCA1–BARD1 interacts with RAD51 directly, and BRCA1 performs several functions at the stalled fork and in double-strand break repair (Zhao et al., 2017). In addition, chromatin immunoprecipitation

sequencing (ChIP-seq) showed that ZSCAN5B binds with the promoter region of *RAD51* (Sun et al., 2016). These results suggest that *Zscan5b* regulates *Rad51* expression and is involved in postdamage DNA repair during mitosis.

Zscan5b Binds to Linker Histone H1 and Protects Chromatin Structure

Immunoprecipitation assays using proteins extracted from ESCs and HeLa cells transfected with *Zscan5b* and vectors expressing histone proteins H1.1, H1.2, and H1.4 showed that the ZSCAN5B protein binds to histones H1.1, H1.2, and H1.4. Hashimoto et al. (2010) reported that the linker protein histone H1 plays an important role in nucleosome spacing and interphase nuclear compaction. In addition, histone H1-null somatic mouse cells show an ~7-fold increase in the rate of chromosomal aberrations, including chromosomal gaps and breaks, compared with wild-type cells (Hashimoto et al., 2010). These results suggest that ZSCAN5B is associated with histone H1 and contributes to the maintenance of chromosomal architecture.

Zscan5b-Deficient Mouse Is a Model of the Human Disease, Chromosome Instability Syndrome

The *Zscan5b*-deficient mouse cannot repair postreplication DNA damage, and shows an increase in chromosome aberrations including gaps, breaks, gain or loss of chromosomes, and Robertsonian translocations. Defective DNA repair is a common feature of chromosome instability syndromes, also known as chromosome breakage syndromes (Sun et al., 2016). The classic chromosome instability syndromes are Fanconi pancytopenia syndrome, Bloom syndrome, and ataxia-telangiectasia. The diagnostic cytogenetic finding in Bloom syndrome is a marked increase in the level of spontaneous sister chromatid exchanges (SCEs). The normal rate of SCEs in human cells is 6–10; however, in Bloom syndrome, more than 50 SCEs per cell are found (Ellis et al., 2001). A Q-banding analysis of *Zscan5b*-deficient spleen cells showed the presence of chromosomal gaps; this phenotype resembles that of some chromosomal instability syndromes. We therefore analyzed SCE frequencies in *Zscan5b*-deficient spleen cells and wild-type somatic cells, but no significant differences in total SCE numbers were found: 8.20 in 18 wild-type cells; 8.35 in 20 *Zscan5b*-deficient somatic cells (Figure S6). The gene for Bloom syndrome, *BLM*, encodes a protein that interacts with RAD51 protein to protect somatic cells against chromosomal aberrations (Sassi et al., 2013). Chromosome analysis showed that most mitotic metaphase cells with *Rad51* deficiency carried isochromatid-type breaks before cell death (Sonoda et al., 1998). ZSCAN5B has been reported to bind to the promoter regions of the tumor suppressor genes *RAD51* and *BRCA1* in ChIP-seq analyses (Sun et al., 2016). *BRCA1*, *BRCA2*, and *RAD51* can suppress an aberrant replicative homologous recombination response at stalled forks (Willis et al., 2017). Our microarray data showed elevated expression of *Rad51l3* and *Bard1* in *Zscan5b*-deficient ESCs, implying that *Zscan5b* performs several functions as a transcription factor and in DNA double-strand break repair through interaction with these tumor suppressor genes. In addition, COSMIC (the Catalogue of Somatic Mutations in Cancer) (http://www.sanger.ac.uk/cosmic) indicates that mutation of the orthologous human gene *ZSCAN5B* occurs in ovarian cancer (COSP26515, COSU331), lung cancer (COSU418), and Fanconi anemia (COSP39462). Therefore, we propose that the *Zscan5b*-deficient mouse could be used as a model of chromosome breakage syndromes, and would be useful for exploring their origin and for developing treatment therapies.

Conclusion

To our knowledge, this is the first report showing that the ZGA gene *Zscan5b* is involved in the maintenance of genomic integrity during mitosis. We propose that abnormal mitosis without the presence of *Zscan5b* induces genome instability and causes altered stem cell differentiation leading to tumorigenesis. In addition, *Zscan5b* might be involved in maintaining DNA structure in combination with histone H1 and for packaging chromosomes into a high order of chromatin structure to prevent chromosomal abnormalities. Testing this hypothesis will be carried out in subsequent investigations.

EXPERIMENTAL PROCEDURES

Identification of the Mouse Zscan5b Gene by *In Silico* Analysis

Preimplantation-specific genes were identified by global gene expression profiling of oocytes and preimplantation embryos (Hamatani et al., 2004) and EST frequencies in the Unigene database. SMART (Schultz et al., 1998) was used for domain prediction analysis.

Collection and Manipulation of Oocytes

Female B6D2F$_1$ mice were superovulated at 6–8 weeks old by injection of 5 IU of pregnant mare serum gonadotropin (Sigma-Aldrich, St Louis, MO, USA), followed 48 h later by 5 IU of hCG (Sigma-Aldrich). Unfertilized eggs were harvested 18 h after the hCG injection by the standard method (Nagy et al., 2003), and cumulus cells were removed by incubation in M2 medium (EmbryoMax M2 Powdered Mouse Embryo Culture Medium; Millipore, Billerica, MA, USA) supplemented with 300 mg/mL hyaluronidase (Sigma-Aldrich). The eggs were then thoroughly washed, selected for good morphology, and collected. Fertilized eggs were also harvested from mated superovulated mice in the same way as unfertilized eggs; embryos with two pronuclei were collected to synchronize *in vitro* embryo development. Fertilized eggs were cultured in synthetic oviductal medium enriched with potassium

(EmbryoMax KSOM Powdered Mouse Embryo Culture Medium; Millipore) at 37°C in an atmosphere of 95% air/5% CO_2. Cultured blastocysts were transferred into the uteri of 2.5 d.p.c. (day post coitum) pseudopregnant ICR female mice as described previously (Nagy et al., 2003).

Ethical Approval for the Use of Animals

The Institutional Review Board of the National Research Institute for Child Health and Development (NRICHD, approval number A2006-009), Japan and of Keio University (approval number 10240-(1)) granted ethical approval for oocyte and embryo collection from the mice.

Blastocyst Outgrowth and ESC Isolation

The zona pellucida of blastocysts at 3.5 d.p.c. was removed using acidic Tyrode's solution (Sigma). The blastocysts were cultured individually in ES medium: KnockOut DMEM (Invitrogen) containing 15% KnockOut Serum Replacement (Invitrogen), 2,000 U/mL ESGRO (mouse leukemia inhibitory factor [mLIF]; Chemicon, Temecula, CA, USA), 0.1 mM nonessential amino acids, 2 mM GlutaMax (Invitrogen), 0.1 mM β-mercaptoethanol (Invitrogen), and penicillin/streptomycin (50 U/50 mg/mL; Invitrogen) on irradiated mouse embryonic fibroblast (MEF) cells at 37°C in an atmosphere of 5% CO_2 according to a standard procedure (Nagy et al., 2003). The cultured cells were examined and photographed daily. After 1 week, proliferating cells were trypsinized using Accutase (Invitrogen), and passaged onto new MEF plates. After two more passages, mouse ESC lines were isolated.

Blastocyst Injections to Produce Chimeras

To visualize the *in vivo* contribution of *Zscan5b*-deficient ESCs, *Zscan5b*-deficient ESCs were electroporated with the piggyBac transposon gene expression vector and transposase-expressing vector using a 4D-nucleofector device (Ikawa et al., 1999). We isolated the GFP-positive *Zscan5b*-deficient ESCs (EGFP-*Zscan5b*-deficient ESCs) line, which was continuously cultured on feeder layers in mouse ESC medium with LIF. EGFP-*Zscan5b*-deficient ESCs were injected into blastocysts of B6D2F1 mice, then transferred to the uteri of pseudopregnant ICR mice. Embryos were dissected on E14.5 and the contribution of ESCs to embryos was assessed using a fluorescence stereomicroscope (MVX10, OLYMPUS, Japan).

Irradiation

Irradiation of mouse ESCs was performed as previously described (Fukawatase et al., 2014). In brief, cells were given 4 Gy of X-rays, using a CELLRAD (Faxitron Bioptics, Tuscon, AZ, USA). Immediately after irradiation, cells were returned to the incubator at 37°C in a humidified atmosphere containing 95% air and 5% CO_2, and incubated until further processing. Cell numbers were counted using a TC20 automated cell counter (Bio-Rad Laboratories, Hercules, CA, USA).

Transfection with Zscan5b Constitutive Expression Plasmid

Zscan5b-deficient ESCs were washed with PBS once, detached by Accutase and suspended in ESC derivation medium. Cells were dissociated into a single-cell suspension by vigorous pipetting and counted. Pellets were made and mixed with 1 μg of transposase-expressing vector and 1 μg of the piggyBac transposon gene expression vector (pPB-CAG-mZscan5b-P2A-EGFP) (Niwa et al., 1991) purchased from VectorBuilder in 100 μL of P2 primary cell nucleofector solution (Lonza, Switzerland). The cell suspension was transferred to a cuvette and electroporated using a 4D-nucleofector device (Lonza) with program CG-104 following the manufacturer's protocol. The electroporated cells were plated onto a six-well plate on MEF in mouse ESC medium. The GFP-positive colonies were picked up and the clonal lines were maintained as rescued *Zscan5b*-deficient mouse ESCs (res-Zscan5b-deficient ESCs).

Statistical Analysis

A chi-square test or a one-way ANOVA with Bonferroni's multiple comparison testing was used for statistical analyses. Statistical analyses were performed using GraphPad Prism software (GraphPad, San Diego, CA, USA). $p < 0.05$ was considered to indicate statistical significance (*$p < 0.05$, ****$p < 0.0001$).

ACCESSION NUMBERS

The GEO accession number for the data reported in this paper are GSE124354.

SUPPLEMENTAL INFORMATION

Supplemental Information can be found online at https://doi.org/10.1016/j.stemcr.2019.05.002.

AUTHOR CONTRIBUTIONS

S.O., M.Y., and T.H. designed the study, and performed the data analysis and interpretation with K.M., Y.Y., M.T., and A.U. M.Y. wrote the manuscript with input from all authors. S.O., Akihiro Nakamura, M.Y., R. Ooka, and R. Okawa performed gene expression analysis. H.T. performed the knockout analysis. S.O. derived the ESCs, and performed characterization and differentiation of ESCs with assistance from M.Y., Akari Nakamura, and H.A. J.M. and A.U. performed and interpreted the pathological analysis. T.S. and Akari Nakamura performed the rescue analysis. S.M. and Akari Nakamura produced chimeras. S.O., M.Y., and T.H. performed the microarray analysis. M.Y. performed the statistical analysis.

ACKNOWLEDGMENTS

We are grateful to Hideki Tsumura and the staff of the Animal Care Facility at NRICHD and Keio University for mouse husbandry, the Collaborative Research Resources of Keio University for technical support and reagents, and to Erika Suzuki and Tomoyuki Kawasaki for help with editing the figures. All authors read and approved the final manuscript. This work was supported, in part, by a National Grant-in-Aid from the Japanese Ministry of Health, Labour and Welfare (NCCHD24-6 to T.H. and H.A.), a Grant-in-Aid from the Japan Health Sciences Foundation (KHD1220 to T.H. and H.A.), the Kanae Foundation (to M.Y.), the Takeda Science Foundation (to M.Y.), Grants-in-Aid from the Japan Society for the Promotion

of Science (Kiban-B-25293345 and Kiban-B-16H05475 to T.H., Wakate-B-23791862 to S.O., and Wakate-A-17H05100 to M.Y.).

Received: June 1, 2018
Revised: May 1, 2019
Accepted: May 2, 2019
Published: May 30, 2019

REFERENCES

Balajee, A.S., and Geard, C.R. (2004). Replication protein A and gamma-H2AX foci assembly is triggered by cellular response to DNA double-strand breaks. Exp. Cell Res. *300*, 320–334.

Boroviak, T., Stirparo, G.G., Dietmann, S., Hernando-Herraez, I., Mohammed, H., Reik, W., Smith, A., Sasaki, E., Nichols, J., and Bertone, P. (2018). Single cell transcriptome analysis of human, marmoset and mouse embryos reveals common and divergent features of preimplantation development. Development *145*. https://doi.org/10.1242/dev.167833.

Capalbo, A., Bono, S., Spizzichino, L., Biricik, A., Baldi, M., Colamaria, S., Ubaldi, F.M., Rienzi, L., and Fiorentino, F. (2013). Sequential comprehensive chromosome analysis on polar bodies, blastomeres and trophoblast: insights into female meiotic errors and chromosomal segregation in the preimplantation window of embryo development. Hum. Reprod. *28*, 509–518.

Daphnis, D.D., Fragouli, E., Economou, K., Jerkovic, S., Craft, I.L., Delhanty, J.D., and Harper, J.C. (2008). Analysis of the evolution of chromosome abnormalities in human embryos from day 3 to 5 using CGH and FISH. Mol. Hum. Reprod. *14*, 117–125.

Demko, Z.P., Simon, A.L., McCoy, R.C., Petrov, D.A., and Rabinowitz, M. (2016). Effects of maternal age on euploidy rates in a large cohort of embryos analyzed with 24-chromosome single-nucleotide polymorphism-based preimplantation genetic screening. Fertil. Steril. *105*, 1307–1313.

Edelstein, L.C., and Collins, T. (2005). The SCAN domain family of zinc finger transcription factors. Gene *359*, 1–17.

Egli, D., Birkhoff, G., and Eggan, K. (2008). Mediators of reprogramming: transcription factors and transitions through mitosis. Nat. Rev. Mol. Cell Biol. *9*, 505–516.

Ellis, N.A., Ciocci, S., and German, J. (2001). Back mutation can produce phenotype reversion in Bloom syndrome somatic cells. Hum. Genet. *108*, 167–173.

Falco, G., Stanghellini, I., and Ko, M.S. (2006). Use of Chuk as an internal standard suitable for quantitative RT-PCR in mouse preimplantation embryos. Reprod. Biomed. Online *13*, 394–403.

Falco, G., Lee, S.L., Stanghellini, I., Bassey, U.C., Hamatani, T., and Ko, M.S. (2007). Zscan4: a novel gene expressed exclusively in late 2-cell embryos and embryonic stem cells. Dev. Biol. *307*, 539–550.

Forget, A.L., and Kowalczykowski, S.C. (2010). Single-molecule imaging brings Rad51 nucleoprotein filaments into focus. Trends Cell Biol. *20*, 269–276.

Fukawatase, Y., Toyoda, M., Okamura, K., Nakamura, K., Nakabayashi, K., Takada, S., Yamazaki-Inoue, M., Masuda, A., Nasu, M., Hata, K., et al. (2014). Ataxia telangiectasia derived iPS cells show preserved X-ray sensitivity and decreased chromosomal instability. Sci. Rep. *4*, 5421.

Hamatani, T., Carter, M.G., Sharov, A.A., and Ko, M.S. (2004). Dynamics of global gene expression changes during mouse preimplantation development. Dev. Cell *6*, 117–131.

Harper, J.C., Coonen, E., Handyside, A.H., Winston, R.M., Hopman, A.H., and Delhanty, J.D. (1995). Mosaicism of autosomes and sex chromosomes in morphologically normal, monospermic preimplantation human embryos. Prenat. Diagn. *15*, 41–49.

Hashimoto, H., Takami, Y., Sonoda, E., Iwasaki, T., Iwano, H., Tachibana, M., Takeda, S., Nakayama, T., Kimura, H., and Shinkai, Y. (2010). Histone H1 null vertebrate cells exhibit altered nucleosome architecture. Nucleic Acids Res. *38*, 3533–3545.

Hassold, T., and Hunt, P. (2001). To err (meiotically) is human: the genesis of human aneuploidy. Nat. Rev. Genet. *2*, 280–291.

Ikawa, M., Yamada, S., Nakanishi, T., and Okabe, M. (1999). Green fluorescent protein (GFP) as a vital marker in mammals. Curr. Top. Dev. Biol. *44*, 1–20.

Kort, D.H., Chia, G., Treff, N.R., Tanaka, A.J., Xing, T., Vensand, L.B., Micucci, S., Prosser, R., Lobo, R.A., Sauer, M.V., et al. (2016). Human embryos commonly form abnormal nuclei during development: a mechanism of DNA damage, embryonic aneuploidy, and developmental arrest. Hum. Reprod. *31*, 312–323.

Kosugi, S., Hasebe, M., Tomita, M., and Yanagawa, H. (2009). Systematic identification of cell cycle-dependent yeast nucleocytoplasmic shuttling proteins by prediction of composite motifs. Proc. Natl. Acad. Sci. U S A *106*, 10171–10176.

Mamo, S., Gal, A.B., Bodo, S., and Dinnyes, A. (2007). Quantitative evaluation and selection of reference genes in mouse oocytes and embryos cultured in vivo and in vitro. BMC Dev. Biol. *7*, 14.

McCoy, R.C. (2017). Mosaicism in preimplantation human embryos: when chromosomal abnormalities are the norm. Trends Genet. *33*, 448–463.

McCoy, R.C., Demko, Z.P., Ryan, A., Banjevic, M., Hill, M., Sigurjonsson, S., Rabinowitz, M., and Petrov, D.A. (2015). Evidence of selection against complex mitotic-origin aneuploidy during preimplantation development. PLoS Genet. *11*, e1005601.

Nagy, A., Gertsenstein, M., Vintersten, K., and Behringer, R. (2003). Manipulating the Mouse Embryo: A Laboratory Manual, Third Edition (Cold Spring Harbor Laboratory).

Niwa, H., Yamamura, K., and Miyazaki, J. (1991). Efficient selection for high-expression transfectants with a novel eukaryotic vector. Gene *108*, 193–199.

Noggle, S., Fung, H.L., Gore, A., Martinez, H., Satriani, K.C., Prosser, R., Oum, K., Paull, D., Druckenmiller, S., Freeby, M., et al. (2011). Human oocytes reprogram somatic cells to a pluripotent state. Nature *478*, 70–75.

Rubio, C., Rodrigo, L., Mercader, A., Mateu, E., Buendia, P., Pehlivan, T., Viloria, T., De los Santos, M.J., Simon, C., Remohi, J., et al. (2007). Impact of chromosomal abnormalities on preimplantation embryo development. Prenat. Diagn. *27*, 748–756.

Sassi, A., Popielarski, M., Synowiec, E., Morawiec, Z., and Wozniak, K. (2013). BLM and RAD51 genes polymorphism and susceptibility to breast cancer. Pathol. Oncol. Res. *19*, 451–459.

Schmitges, F.W., Radovani, E., Najafabadi, H.S., Barazandeh, M., Campitelli, L.F., Yin, Y., Jolma, A., Zhong, G., Guo, H.,

Kanagalingam, T., et al. (2016). Multiparameter functional diversity of human C2H2 zinc finger proteins. Genome Res. *26*, 1742–1752.

Schultz, J., Milpetz, F., Bork, P., and Ponting, C.P. (1998). SMART, a simple modular architecture research tool: identification of signaling domains. Proc. Natl. Acad. Sci. U S A *95*, 5857–5864.

Skamagki, M., Correia, C., Yeung, P., Baslan, T., Beck, S., Zhang, C., Ross, C.A., Dang, L., Liu, Z., Giunta, S., et al. (2017). ZSCAN10 expression corrects the genomic instability of iPSCs from aged donors. Nat. Cell Biol. *19*, 1037–1048.

Sonoda, E., Sasaki, M.S., Buerstedde, J.M., Bezzubova, O., Shinohara, A., Ogawa, H., Takata, M., Yamaguchi-Iwai, Y., and Takeda, S. (1998). Rad51-deficient vertebrate cells accumulate chromosomal breaks prior to cell death. EMBO J. *17*, 598–608.

Sun, Y., Zhang, H., Kazemian, M., Troy, J.M., Seward, C., Lu, X., and Stubbs, L. (2016). ZSCAN5B and primate-specific paralogs bind RNA polymerase III genes and extra-TFIIIC (ETC) sites to modulate mitotic progression. Oncotarget *7*, 72571–72592.

van Gent, D.C., Hoeijmakers, J.H., and Kanaar, R. (2001). Chromosomal stability and the DNA double-stranded break connection. Nat. Rev. Genet. *2*, 196–206.

Vanneste, E., Voet, T., Le Caignec, C., Ampe, M., Konings, P., Melotte, C., Debrock, S., Amyere, M., Vikkula, M., Schuit, F., et al. (2009). Chromosome instability is common in human cleavage-stage embryos. Nat. Med. *15*, 577–583.

Wang, Q.T., Piotrowska, K., Ciemerych, M.A., Milenkovic, L., Scott, M.P., Davis, R.W., and Zernicka-Goetz, M. (2004). A genome-wide study of gene activity reveals developmental signaling pathways in the preimplantation mouse embryo. Dev. Cell *6*, 133–144.

Willis, N.A., Frock, R.L., Menghi, F., Duffey, E.E., Panday, A., Camacho, V., Hasty, E.P., Liu, E.T., Alt, F.W., and Scully, R. (2017). Mechanism of tandem duplication formation in BRCA1-mutant cells. Nature *551*, 590–595.

Yamada, M., Hamatani, T., Akutsu, H., Chikazawa, N., Kuji, N., Yoshimura, Y., and Umezawa, A. (2010). Involvement of a novel preimplantation-specific gene encoding the high mobility group box protein Hmgpi in early embryonic development. Hum. Mol. Genet. *19*, 480–493.

Yamada, M., Johannesson, B., Sagi, I., Burnett, L.C., Kort, D.H., Prosser, R.W., Paull, D., Nestor, M.W., Freeby, M., Greenberg, E., et al. (2014). Human oocytes reprogram adult somatic nuclei of a type 1 diabetic to diploid pluripotent stem cells. Nature *510*, 533–536.

Zalzman, M., Falco, G., Sharova, L.V., Nishiyama, A., Thomas, M., Lee, S.L., Stagg, C.A., Hoang, H.G., Yang, H.T., Indig, F.E., et al. (2010). Zscan4 regulates telomere elongation and genomic stability in ES cells. Nature *464*, 858–863.

Zhao, W., Steinfeld, J.B., Liang, F., Chen, X., Maranon, D.G., Jian Ma, C., Kwon, Y., Rao, T., Wang, W., Sheng, C., et al. (2017). BRCA1–BARD1 promotes RAD51-mediated homologous DNA pairing. Nature *550*, 360–365.